Motion in a Particle Bed Agitated by a Single Blade

B. F. C. Laurent and J. Bridgwater
Dept. of Chemical Engineering, University of Cambridge, Pembroke Street, Cambridge, CB2 3RA, U.K.

D. J. Parker
Positron Imaging Centre, School of Physics and Astronomy, The University of Birmingham, Birmingham, B15 2TT, U.K.

Studies on the agitation of granular materials were conducted in a horizontal cylindrical shell stirred by a single long flat blade located on radial arms fixed to a rotor shaft. Positron emission particle tracking, a noninvasive method of investigating opaque systems, permitted the motion of a single particle to be followed. Axial flow patterns showed two loops of circulation inside each compartment defined by the radial arms of the rotating blades. Results revealed the presence at 20% of fill of a circulation zone in the cross-sectional plane directly beneath the rotating shaft where little agitation occurred. This zone decreased in size and moved toward the agitator shaft as fill increased from 20% to 60%. Velocity profiles and Fourier analysis of particle displacement showed that particle movement was controlled by the number of blade passes. Torque measurements on the agitator shaft were correlated with distribution of material in the cross section of the mixer and distribution of tangential velocity. This opens the prospect of relating torque to powder flow patterns. The information can now be incorporated into models for heat transfer, chemical reaction, or agglomeration.

Introduction

The mixing of powders by mechanical-driven stirrers is common in processing. The purpose may be to improve homogeneity, to promote heat transfer or drying, to influence chemical reaction, to cause agglomeration or to cause particle breakage. The need arises in many processes in many industries. The mechanisms generating particle motion and shear are not at all well understood, however, the state of knowledge being markedly inferior to that pertaining to gases or liquids. The influences of material and process parameters are not at all well known either in the laboratory scale or the industrial scale.

The traditional approach to powder mixing is well summarized in the survey by Poux et al. (1991). The mixer is operated, samples withdrawn and analyzed, and some arbitrary function of the variance of sample concentration used to describe the system. For instance, Müller and Rumpf (1967) developed a model based on such an approach and applied it to experiments in a ploughshare mixer. Due to a lack of appropriate experimental techniques, however, the development of models describing particle flow patterns has not been possible until now, and thus existing models are of very limited value.

There are a few notable recent exceptions; these researchers are finally developing significant scientific insights into powder mixing. Thus, Malhotra and Mujumdar (1990) viewed a cylindrical stirred system through one end wall and interpreted their findings in relation to particle motion in the vicinity of the blade. In 1995, McCarthy et al. developed a theory of the powder behavior in rotary drums. Metcalfe et al. (1998) provided some insights into powder flow in the cross section of a rotating cylinder using MRI. Moakher et al. (2000) presented a comparative study between experimental results in tumbling blenders and results given by a discrete element model. Powder mixing mechanisms have been described using chaos theory. The work of Shinbrot et al. (1999) and of Khakhar et al. (1999) provide illustrations of this approach.

Correspondence concerning this article should be addressed to B. F. C. Laurent.

In 1997, Parker et al. reported studies of internal motion in rotary horizontal drums using a positron camera. The first use of a positron camera for mechanically stirred systems is reported in the work of Broadbent et al. (1993).

Positron emission tomography (PET), originally developed for medical purposes, is a noninvasive technique used recently to investigate solid or liquid systems. In this work, the particular technique used is positron emission particle tracking (PEPT). The motion of a single positron-emitting particle is followed, and the technique yields spatial coordinates of this tracer as a function of time. Particles can be followed up to 2 m/s in equipment of up to 400 mm in diameter. This method permits the investigation of powder mixing with more certainty than methods based on physical sampling that are tedious and easily induce systematic errors. PEPT also provides qualitative and quantitative information on internal flow-patterns. Its capabilities and applications for powder mixers have been shown by Parker et al. (1993) and Broadbent et al. (1993). Three-dimensional bulk-density maps may be calculated, whereas techniques such as sampling or injection of tracer provide information on external aspects of the mixing process quantified by a standard deviation of concentration or a residence time distribution. Finally, the PEPT data files give flexibility for analysis.

The studies arose from a need to understand the mode of operation of a multiblade mixer. The abstraction of a single blade gave rise to the issues here. The behavior of a multiblade mixer and how it relates to the present work will be reported in the future. The present purpose is thus to provide a detailed description of particle flow over a single blade.

Experimental Method

Positron-emitting particles are made labeled with an isotope having a proton-rich nucleus that induces a positron decay. The tracer used here is in the form of porous resin beads of diameter 600 μm and density 1 kg/L. The active radionucleide is ^{18}F, a positron emitter of half-life 110 mn, enabling typically 4 h of experiments. It is produced by placing water in a cyclotron that yields a beam of ^{3}He ions, activating the oxygen in the water through the reactions ^{16}O(^{3}He, p) ^{18}F and ^{16}O(^{3}He, n) ^{18}Ne $\rightarrow$ ^{18}F. The fluoride ions are then adsorbed into the resin particle by ion exchange.

A positron emitted by a nucleus annihilates with an electron within 2 mm with a probability of over 99% in a material of the density of water. This positron–electron annihilation produces two 511-keV colinear γ-rays that are detected by two detectors, one situated on each side of the tracer. Each detector contains a series of 20 cathode–anode planes with a sensitive area of 600 mm by 300 mm and has an efficiency for detection of γ-rays of 7%. The cathode planes consist of lead strips; the anode planes have a series of parallel tungsten wires. The strips forming the cathode planes are orthogonal to the anode planes so that coordinates are provided after detection of a γ-ray. Due to γ-ray interaction with the lead of a cathode plane by photoelectric absorption or Compton scattering, a fast electron is released into the gas layer situated between two anode–cathode planes. This initiates a so-called Townsend avalanche of electrons that is detected on the adjacent anode plane and its two neighboring cathodes as a voltage pulse. When the data acquisition system is aware of two γ-rays within 20 ns of each other, these are assumed to issue from the same annihilation. This timing resolution is controlled by an electronic clock included in the computer. The location of the impact of the two γ-rays on each of the detectors permits the construction of the line on which the annihilation (termed the event) occurred. In principle, two events give the location of the positron emitter. However, due to γ-ray scattering by interaction with material of the system, for example, some events are corrupted and need to be rejected. An algorithm, fully described by Parker et al. (1993), is used to discriminate true from corrupted events. Over an average of 2000 events per second (including the corrupted events) are processed to give around 50 location points of the tracer per second. These numbers vary with the activity of the tracer. Each location point is stored in the form of the spatial coordinates of the tracer as a function of time. The spatial resolution is approximately 2 mm for a speed of 0.2 m/s and deteriorates with the speed of the tracer, being around 5 mm at a speed of 1 m/s.

The powder had a bulk density of about 0.5 kg/L and a mean diameter of 520 μm. The particle density was around 1 kg/L. Size distribution analysis showed that 80% by mass of the particles had a diameter ranging between 230 and 870 μm. The internal angle of friction was about 30°. The radioactive resin tracer had the same density as the powder and a diameter of 600 μm, close to the mean diameter of the bulk. Both bulk particles and tracer were of spherical shape. These similarities in terms of size, density, and shape ensured that the behavior of the tracer was representative of the behavior of the bulk particles by preventing segregation.

The mixer shell, a torque gauge, and a motor were fixed on a frame. The mixer rotor was connected to the shaft of the motor by a speed reducer and the torque gauge. The detector plates of the positron camera were 600 mm high and of 300-mm horizontal length and were 400 mm apart. This was not sufficient to track the tracer over the whole length (650 mm) of the mixing chamber. The detector plates were thus mounted on horizontal tracks that could be moved along the mixer by a motor. The axial position was directly controlled by the computer used for data acquisition. The particle tracking algorithm estimated the tracer position and optimized the position of the detector plates so that the axial coordinate of the center of the detector plates was as close as possible to the axial position of the tracer. It operated such that, should the tracer move more than 10 cm from the center of the detector plates for more than 0.5 s, the detector plates would move until the axial coordinate of the center of the plate was less than 10 cm from the tracer. This supposed that the axial speed of the tracer was slow compared to that of the detectors, a matter that was verified experimentally. The detector plates did not lose track of the position of the tracer.

Figure 1 shows the mixer, a simplified version of an industrial agitator, of diameter 270 mm and of length 650 mm. Six sets of three radial supports fixed onto the 90-mm-diameter rotor shaft define five axial compartments as the agitator rotates. One of the three sets of radial supports carries a 53-mm-wide flat blade along the length of the mixer. The other two sets were used in related work on multiblades devices. The clearance between the tip of the blade and the inside of the cylindrical shell is 8 mm, while that between an end of the long flat blade and the radial end of the cylinder is 4 mm.

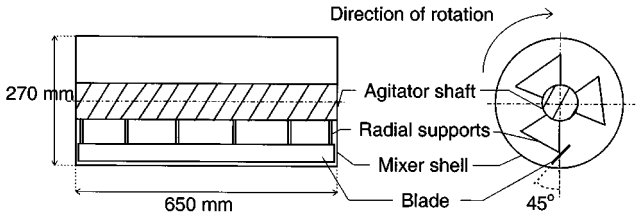

Figure 1. Mixer: side and cross-sectional views.

The blade is inclined to form a 45° angle with the radial direction, as indicated in Figure 1.

The blade position was recorded using an optical transducer and a small iron bar fixed radially on the rotor axis. An electronic clock was used for recording the blade position. Each time the bar passed through the optical transducer (positioned so that it was activated when the blade reached the lower vertical position), an IR beam was interrupted and the electronic clock reset to zero. The acquisition system recorded the time given by the clock. Since the rotation speed was constant, time could be converted into a blade angle.

Results and Discussion

Here we report on the influence of agitator speed (20, 25, 38, and 45 rpm) and the level of fill (20, 30, 40, 50, and 60%). The level of fill is defined by the ratio of the volume of powder in the mixer to the total volume available in the mixing chamber.

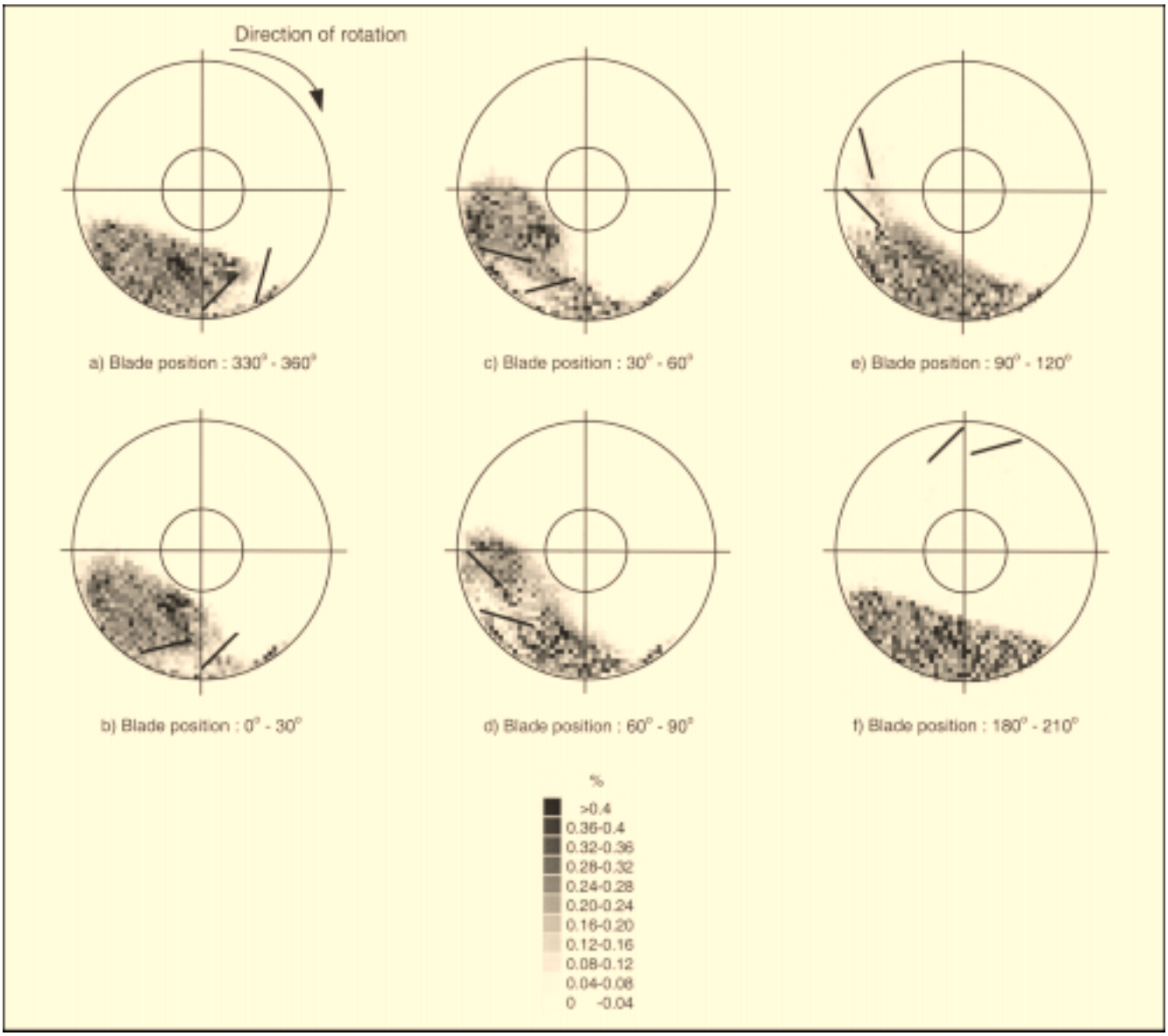

Figure 2. Cross-sectional view of the mixer for six different blade positions.

Level of fill—20%; $N = 38$ rpm.

A case study

The findings are first illustrated from an experiment where the level of fill was 20% and the agitator speed 38 rpm.

Transaxial Flow Patterns. The radial spatial distribution of material is illustrated in Figure 2 for different ranges of blade positions. Each picture shows two limiting blade positions, these defining the data that are selected for analysis. The position is given by the leading edge of the blade, the origin of the angular position being when this leading edge is in the vertical lower position. The PEPT data are broken down according to blade position as follows. A range of blade positions is chosen. The data file containing the data points is read; a data point is considered if the agitator blade corresponding to this point is situated within the range of positions initially selected. The cross-sectional plane of the mixer is divided into a grid of 5-mm-by-5-mm bins, values selected to reveal as much of the detailed structure as possible while having an acceptable number of data points, a value set to a minimum of 20. A smaller bin size causes an inadequate number of data points to report, while a larger bin size fails to discriminate the bulk behavior effectively. The values on the scale give the percentage of time the tracer spends in a given bin.

Figure 2a shows the distribution of material as the blade penetrates into the particle bed. A void created behind the blade is visible in the section behind the blade. Figures 2b and 2c show the change of the surface of the particle bed as the blade pushes material through the bed. An open space exists directly beneath the agitator shaft. The material that has been lifted by the blade flows into this space (Figure 2d). By analogy with the terminology used to describe flow patterns in a rotating drum, the bed may be described as cascading. When the blade is out of the bulk as shown in Figure 2f, the particle bed is at rest, the free surface defining an angle of 15° to the horizontal that is lower than the material angle of repose of 30°.

Figure 3 shows the radial distribution of the tracer integrated over the whole experiment, that is, over all the blade positions. It shows the zone BCEB under the agitator shaft where the probability of occupancy of the tracer is the highest. The two dotted lines drawn in Figure 3 give the position of the free surface when the bed is at rest and when it is cascading, and define two wedges *ABC* and *CDE* of lower probability of the presence of the tracer. McCarthy et al. (1995) investigated particle motion in slowly rotating cylinders. As the cylinder rotates, the angle of the free surface to the horizontal increases and a wedge of the particle bed slips down to the free surface of the bed to a resting position. Certain similarities exist with the present findings, but there is a difference in density between the wedges.

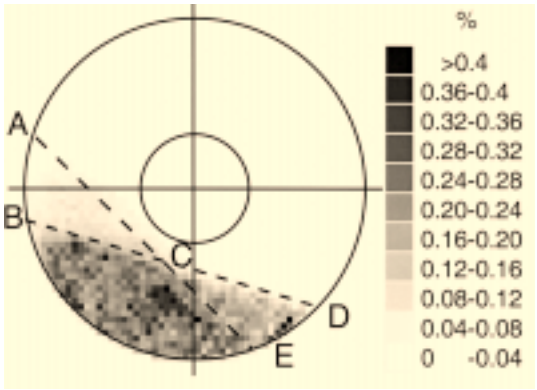

Figure 3. Cross-sectional view of the mixer for all blade positions.

Level of fill—20%; $N = 38$ rpm.

Figure 4 shows the velocity fields for the six ranges of blade position in a way similar to Figure 2. Here the cross-sectional plane is divided into a grid of 10-mm-by-10-mm bins to improve clarity. Within the range of blade positions indicated, the velocity of the tracer is averaged within each bin and represented by an arrow. Figures 4a, 4b, and 4c show different stages of the agitation as the blade moves through the particle bed. A circulation loop appears progressively (Figure 4c) with a center of rotation situated close to the region of high occupancy observed in Figure 3. This zone is situated above the region where the blade passes, in which little agitation occurs. This pattern was observed by Bagster and Bridgwater (1970), who investigated the motion of a single flat blade through a particle bed. They observed that a circulation loop developed in the heap of material in front of the blade. As the blade moves out of the bed (Figures 4d and 4e), the material cascades off the blade and rolls down the free surface. When the blade is completely out of the particle bed, no significant particle motion occurs (Figure 4f).

Profiles of the speed are reported for different ranges of blade positions in a cross-sectional view (Figure 5b). This confirms that the powder is lifted by the blade and starts to flow down on the free surface when the blade is around 30°. Cascading motion on the free surface increases as the blade moves further through the particle bed (Figures 5c and 5d).

These findings can be related to one other piece of work. Malhotra et al. (1988) investigated radial agitation in a cylindrical mixer of diameter 250 mm and of length 150 mm that was stirred by a single paddle. The ratio of the blade height to the bed height was 2, corresponding to a level of fill of about 30%, and the blade speed was 8 rpm. Malhotra et al. looked at the displacement of colored particles via the end wall using a video camera. They observed a stagnant elliptical region situated in the middle of the particle bed above the zone where the blade passes. The size of this zone increased with increase of the ratio of the bed height to the blade height. Maps of trajectories of tracers showed elliptical patterns induced by the blade motion and located around the stagnant zone. Malhotra et al. defined three types of mixing zone in the radial cross section of the mixer: the surface zone where particles cascade and that is around 4 to 8 particle diameters thick; the convective zone in the annular portion of space where the blade passes and where the particles are pushed to the free surface; the zone of little agitation in the center of the bed, where little mixing occurs and where particle trajectories appear to be elliptical streamlines. These features can be seen in the present work.

Axial Flow Patterns. Figure 6a shows the axial displacement of the tracer over a 2000-s period. The two lines in bold at 0 and 650 mm show the axial limits of the mixer. The four other bold lines show the axial position of the radial supports. The dotted lines mark the midpoints between these supports.

Consider the first 300 s of the experiment. The tracer starts at an axial position of 260 mm and is situated in what is termed the second compartment of the mixer, the space between the second and third set of radial supports. It remains inside one half of this compartment for about 180 s before moving into the third compartment. Observation of the axial displacement of the tracer over 2000 s suggests the presence of two circulation loops inside each compartment. The tracer oscillates between the line defining the middle of one compartment and the limit between two adjacent compartments. It is thought that these patterns are generated by the rotating supports. Within 2000 s the tracer jumped fourteen times from one compartment to the next one (at 180, 950, or 1750 s, for example), compared to only three times within a compartment from one half to the other half (at 500, 900, and 1600 s). This suggests that the transfer between two circulation loops within a compartment is more difficult than between two adjacent compartments.

Consider a shorter time period. Figure 6b gives an overview of the axial, radial, and angular displacement of the tracer as a function of time at 38 rpm and a level of fill of 20%. The line at an axial position of 390 mm indicates the axial position of the radial supports between the third and fourth compartments. The tracer follows a pattern of motion in each of the three directions. Consider a typical cycle in the motion of the tracer from $t = 2000$ s. The blade passes into the bed every 1.6 s. At the beginning of the cycle, the tracer is close to the lower part of the free surface. The step in the axial displacement due to a blade pass is associated with a step in the angular and radial displacements of the tracer. The tracer moves inside the particle bed under the motion of the blade, its angular position increasing every time the blade passes through the bulk. When the tracer reaches the free surface of the bed, the angular position then increases rapidly from 60° to about 350°; these angular positions correspond, respectively, to the top and to the bottom of the slope of the free

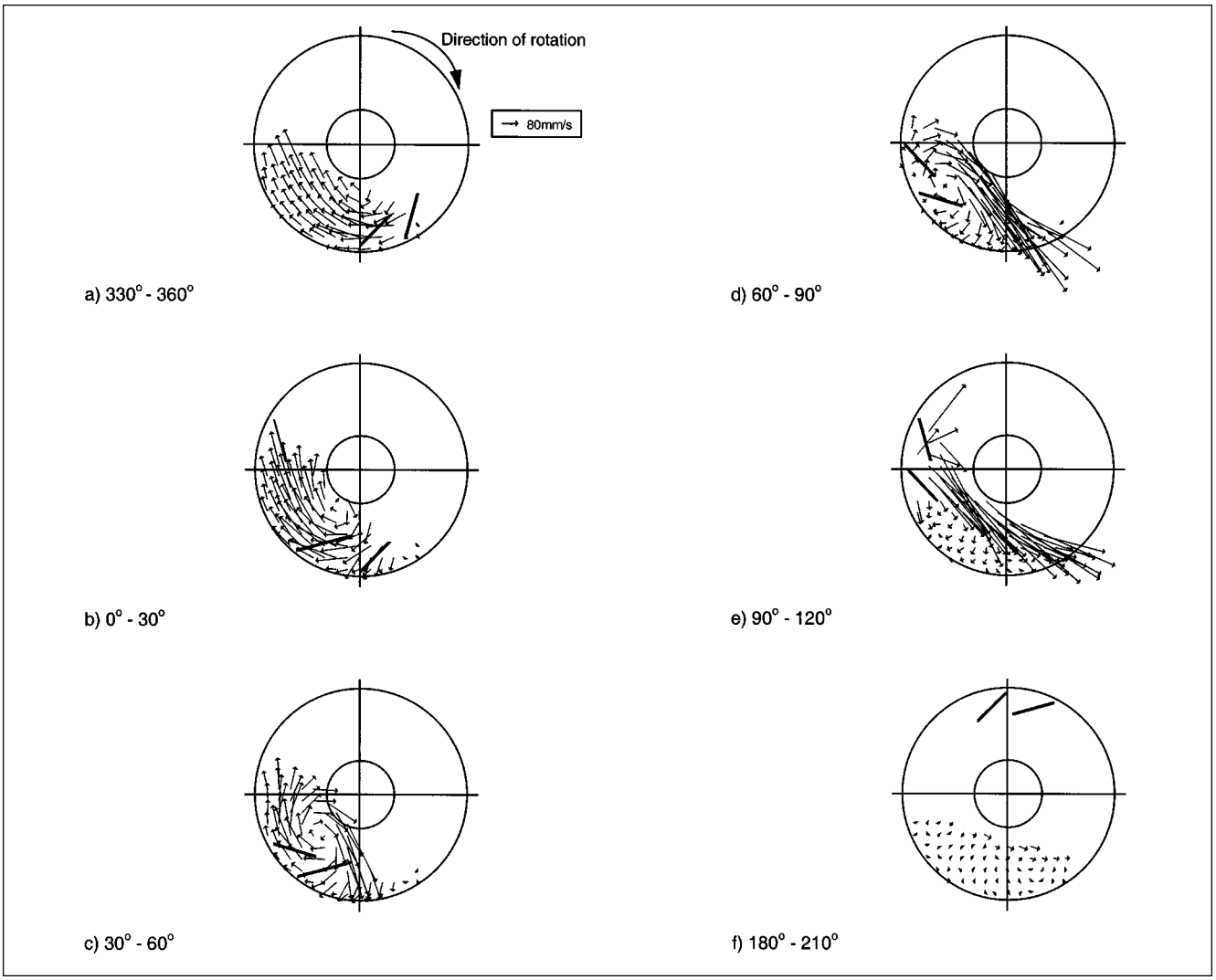

Figure 4. Velocity fields in cross-sectional view for six different blade positions.

Level of fill—20%; $N = 38$ rpm.

surface. During this stage the tracer cascades and flows down onto the free surface. A new cycle then starts. The tracer angular position resets from 360° to 0° every time the tracer passes the lower vertical direction of the cylinder, which produces an apparent jump in the angular position plots that is in fact an artifact of presentation.

The periodicity of this cycle was investigated using a fast Fourier transform of the axial, radial, and angular displacements. All three show peaks at the nondimensional frequency of 1, which corresponds to the rotating speed of the agitator, as well as 2 and 3, which are the harmonics of the dominant peak. Thus the radial, axial, and angular motion are each periodic, the period of the motion being that of the agitator. This corresponds to the impulse given by a blade pass. Another peak appears for angular, axial, and radial displacements at a nondimensional frequency of about 0.25 and is thought to depend on the agitator geometry. The corresponding period of the cycle is around four blade rotations, and corresponds to the phenomenon when the tracer rolls down the surface of the bed. This means approximately four blade passes are needed to bring the tracer from the bottom of the slope to the top. Thus tracer motion is promoted in the three spatial directions when it rolls down on the free surface.

Relationship Between Velocity Distributions and Power Consumption. Figure 7a presents the mean tangential velocity and the torque measured on the agitator shaft vs. the blade position. Between 180° and 270° the blade is out of the particle bed and the tangential velocity is low, since the bed is in a rest state. The blade penetrates the bed and the tangential velocity increases progressively to reach its maximum for a blade position of 0°. The velocity decreases to reach its minimum at a blade position of 90°. As the blade moves further out of the particle bed, the tangential velocity increases and reaches a value close to zero when the bed returns to the rest state shown in Figure 4f. The tracer mean speed shows two maxima, these being formed at blade positions of 0° and 90°. Since the mixer operates in batch mode, the mean radial and axial velocities are zero. It follows that the mean tracer speed is approximately the absolute value of the mean tangential velocity. Hence, the two maxima of the mean speed at a blade position of around 0° and of 90° correspond to the maximum

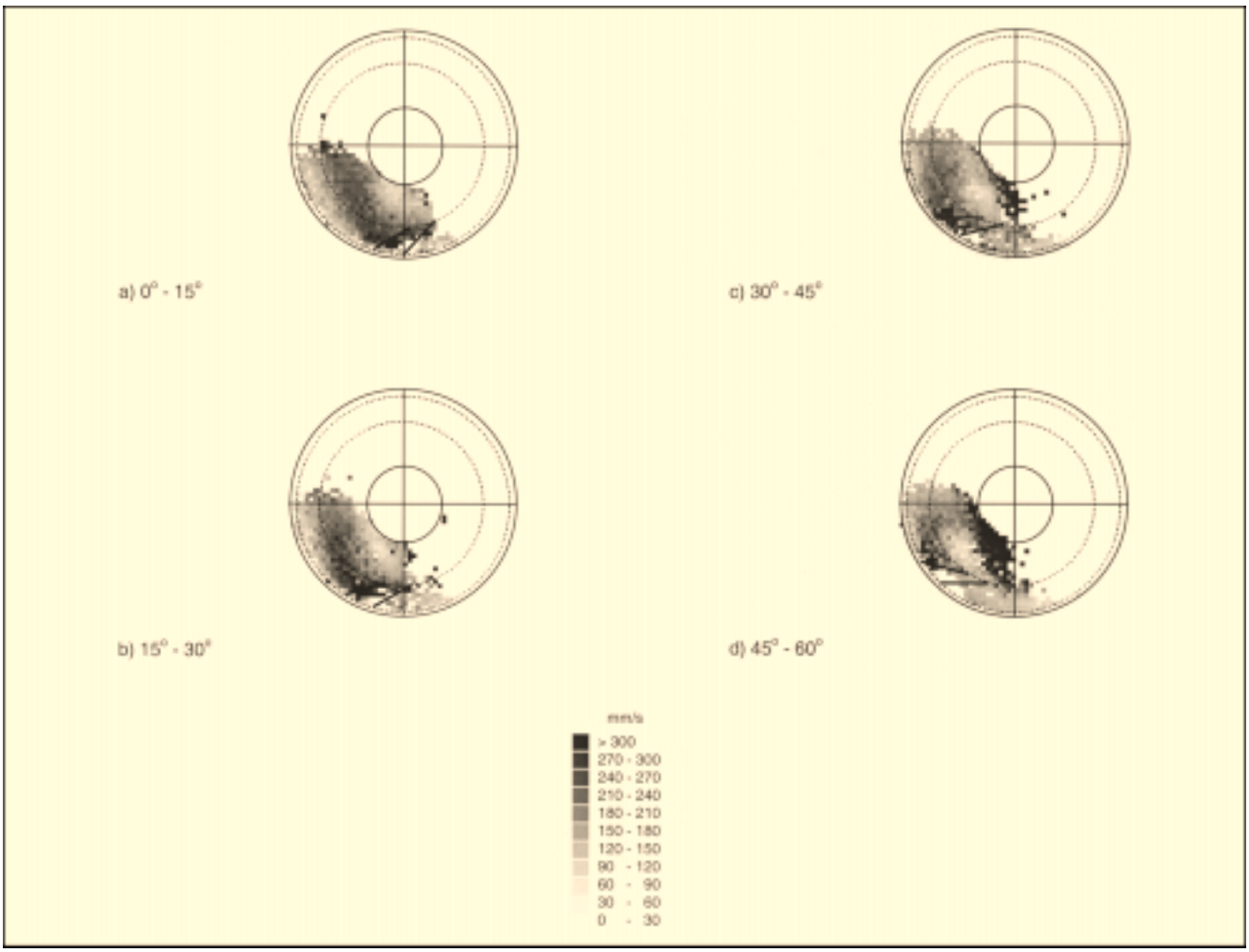

Figure 5. Profiles of the speed for different blade positions.

Cross-sectional view; level of fill—20%; $N = 38$ rpm.

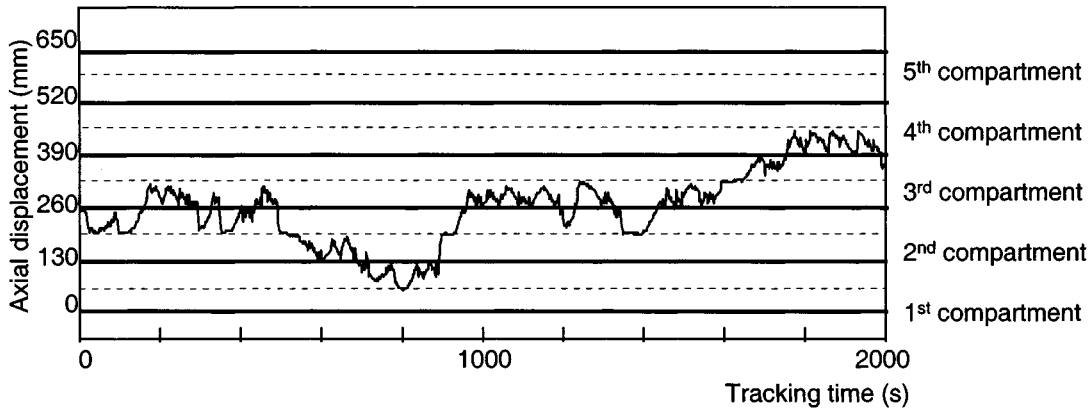

a) Axial displacement of the tracer vs. tracking time

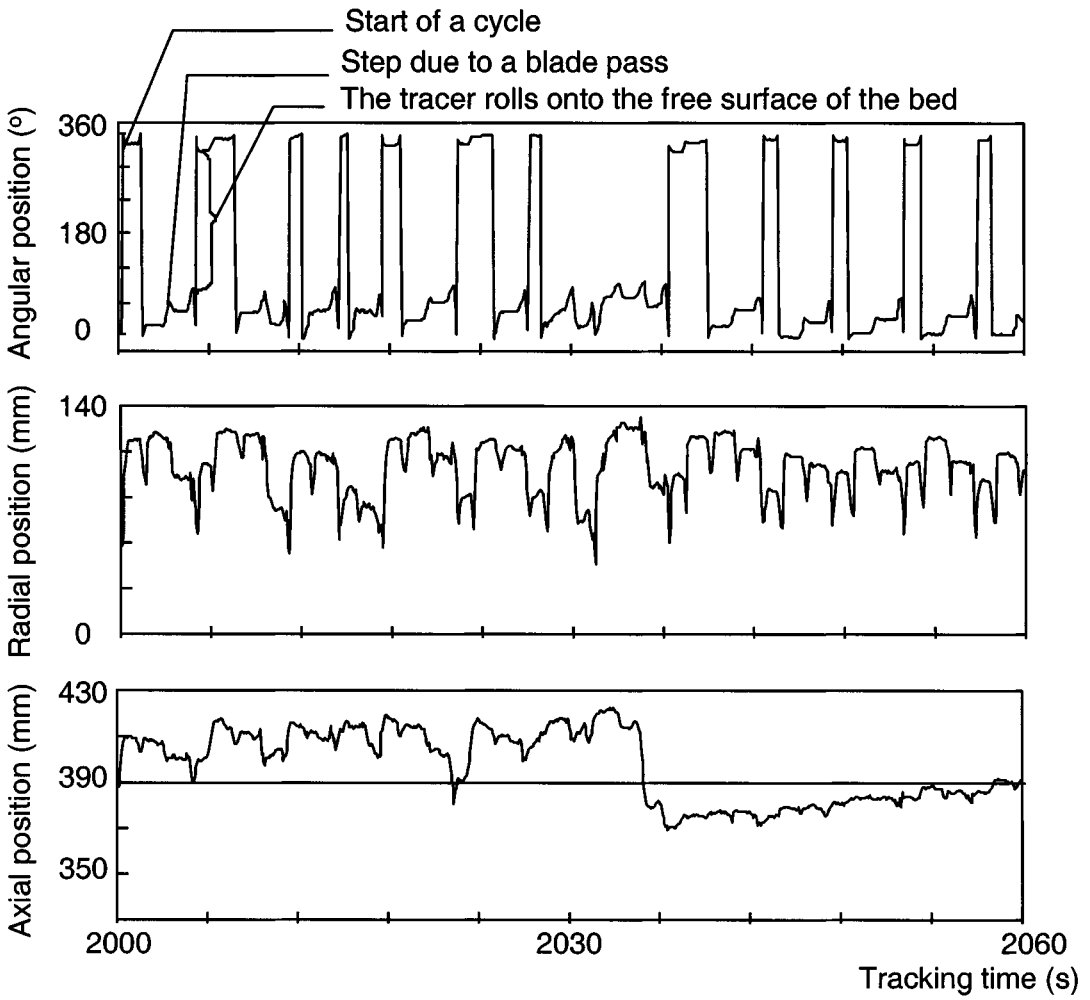

b) Axial, radial and angular displacement of the tracer vs. tracking time.
Note on angular position; the scale shows a step, an artefact of presentation as the tracer progresses from an angle of 360° to 0°.

Figure 6. Displacement of the tracer vs. tracking time.
Level of fill—20%; 38 rpm.

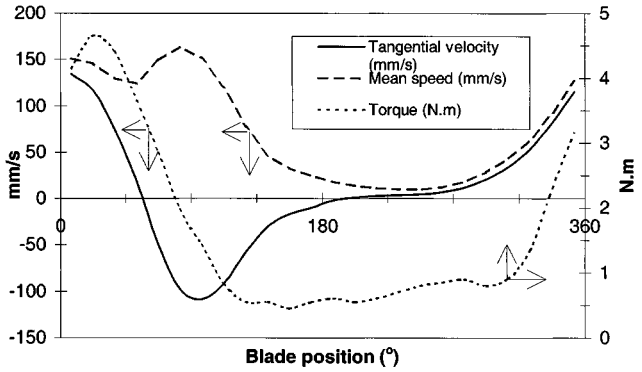

a) Mean tangential velocity, mean speed of the tracer and torque vs. blade position

Level of fill : 20%; N = 38 rpm

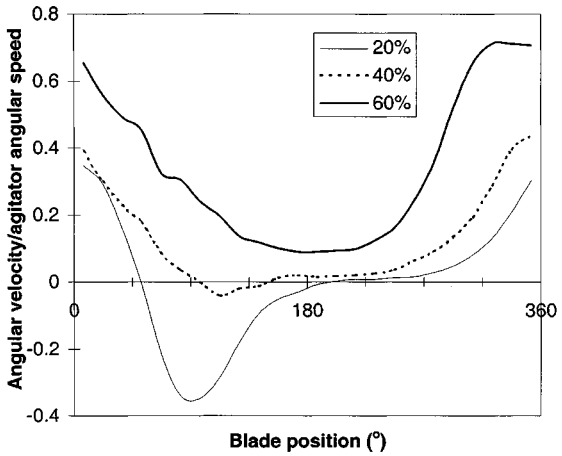

b) Influence of level of fill on the ratio of the mean tracer angular velocity to the agitator angular velocity. N = 38 rpm

Figure 7. Influence of the blade position on the mean angular and tangential velocity.

and the minimum of the mean tangential velocity at a blade position of 0° and 90°, respectively.

Between 180° and 270° the tangential velocity is very low and the bed is at rest, as shown in Figure 4f. Over this angular interval, the torque is low as the blade is out of the particle bed. The signal is then due to the frictional forces at the bearings supporting the rotating shaft together with the torque due to asymmetry of the radial arms and blade (Figure 3), a contribution assumed to be small. As the blade moves into the bulk and reaches 315°, the tangential velocity increases progressively and reaches a maximum when the blade position is around 0°. The torque starts to increase for a blade position of 315° as the blade enters into the particle bed, which is in agreement with the approximate position of the lower point of the free surface estimated in Figure 2f. The slight increase in the torque and tangential velocity for a blade position between 225° and 300° corresponds to the motion of the radial supports of the agitator, which are thought to create some disturbance in the bed. The torque increases further as the blade moves through the bulk, and reaches a maximum when the blade position is 30°. This can be related to Figure 2c, showing how part of the bed is lifted by the blade. The maximum in the torque occurs when all the material is being lifted by the blade before it cascades into the void behind the blade. As material cascades down the free surface of the bed, less material is lifted by the blade and the torque decreases; the tangential velocity becomes negative since, at this level of fill, material is flowing down the free surface in an anticlockwise direction below the center of the agitator. As the blade moves out of the bulk, the mean tangential velocity reaches a minimum. Most of the motion in the bed then occurs at the free surface, Figure 4e. Since the blade is completely out of the particle bed, the torque is low and the mean tangential velocity increases to reach a value close to zero. This is in agreement with Figure 4f, which shows low velocity fields within the particle bed. This phase brings the bed back to its initial state.

This is consistent with observations made by Malhotra and Mujumdar (1990), who monitored the torque on the shaft of a single-blade agitator that operated at 20% fill. They observed that the torque reached a maximum when the blade was engaged in the particle bed to a third of the circumferential length from the bottom of the free surface.

Level of fill

Consider the powder flow patterns in the cross-sectional plane as the blade progresses through the bed where the level of fill is 60% (Figure 8). The position of the free surface is more difficult to evaluate, since the central shaft now interferes with the free surface. As the blade is just about to penetrate the particle bed, the free surface forms an angle of approximately 20° with the horizontal (see the dotted line in Figure 8a). As the blade progresses further into the particle bed, the material is pushed in the annular space between the agitator shaft and the mixer shell as a plug (Figure 8b). No material flows over the shaft and the free surface forms an angle of around 50° with the horizontal. For a blade position between 30° and 60° (Figure 8c), material then flows over the agitator shaft and cascades in the free-fall zone at the right side of the shaft. A void appears immediately under the agitator shaft. This void remains close to the blade as the blade rotates further (Figures 8d and 8e). Once the blade is out of the bed, the bed retains its initial rest position.

Figure 9 shows the profiles of the speed for different blade positions for a level of fill of 60%. Figures 9b and 9c show that the powder begins to flow over the agitator shaft when the blade position is around 330°. As the blade progresses through the particle bed, the speeds in the zone situated between the agitator shaft and the locus of the rear of the blade are significantly lower than those in the zone where the blade passes. This is particularly visible for the zone directly beneath the agitator shaft, where speeds can be a third of those in the region where the powder is pushed directly forward by the blade.

Figure 10 presents velocity fields in cross-sectional view for four levels of fill, the range of blade positions being the same for each level of fill. This range of blade positions was chosen so that the agitator blade was totally immersed in the particle bed at a low level of fill (Figure 2c). A circulation loop is visible beneath the agitator shaft at lower levels of fill, since a significant part of material flows underneath the agitator

shaft. The center of rotation of the circulation zone moves toward the center of the agitator's rotation as the level of fill increases and more material flows over the rotating shaft. For a level of fill of 20%, between a blade position of 60° and 150°, the ratio of the mean angular velocity of the tracer to the agitator angular velocity is negative (Figure 7b), which means that most of the particle bed flows in the opposite direction to that of rotation, that is, underneath the agitator shaft, as observed in Figures 4d and 4e. At higher levels of fill, this ratio is always positive, which is consistent with material of the bulk flowing over the rotating shaft (Figure 10d).

The power function of the Fourier transform of the axial displacement was used to investigate the influence of fill on the tracer displacement. At 60% of fill, a peak at 1 is observed, corresponding to the rotation frequency of the blade, as well as to subsequent harmonic peaks at 2 and 3. The peak corresponding to the frequency of circulation of the tracer from the bottom of the slope of the free surface to its top is around 0.33 (harmonics arise at 0.66, 1, 1.33, etc.) at 60% of fill. This means the average period of circulation of the tracer is now three blade rotations.

Figure 11 summarizes the sequences of the time-periodic flows in the transaxial plane for 20% and for 60% of fill. In each case, the entry of the blade promotes a pushing action on the bed. There is also a cascading on the free surface. For 60% fill, however, as the blade progresses into the bed, most of the material flows over the agitator shaft. The loop of circulation observed at 20% fill still remains at 60% fill, its size having decreased.

Agitator speed

Figure 12 shows that the ratio of the mean angular velocity of the tracer to the agitator angular velocity is independent of agitator speed. The agitator speed was varied from 20 rpm to 45 rpm, which corresponds to a Froude number varying

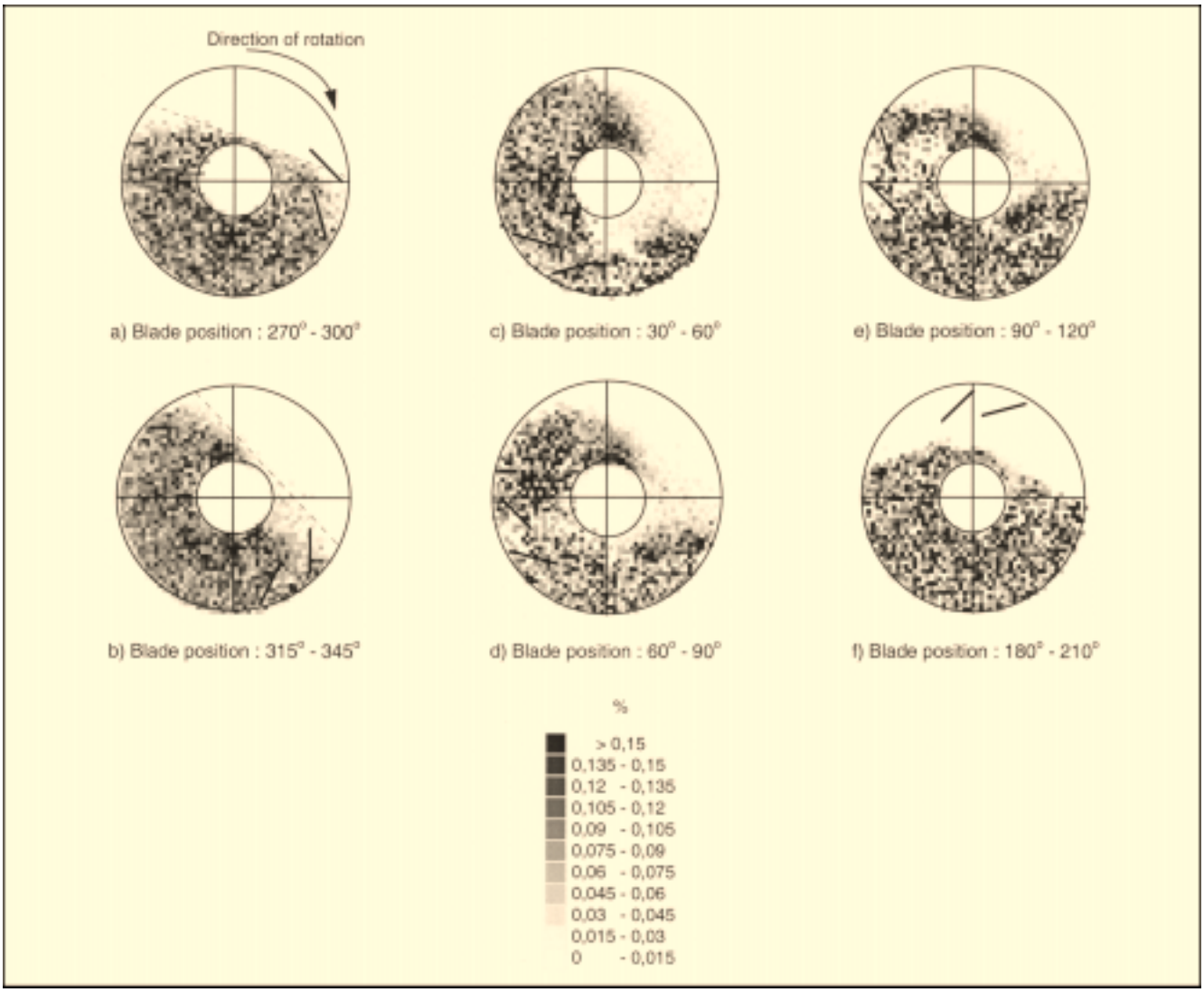

Figure 8. Cross-sectional view of the mixer for six different blade positions.

Level of fill—60%; $N = 38$ rpm.

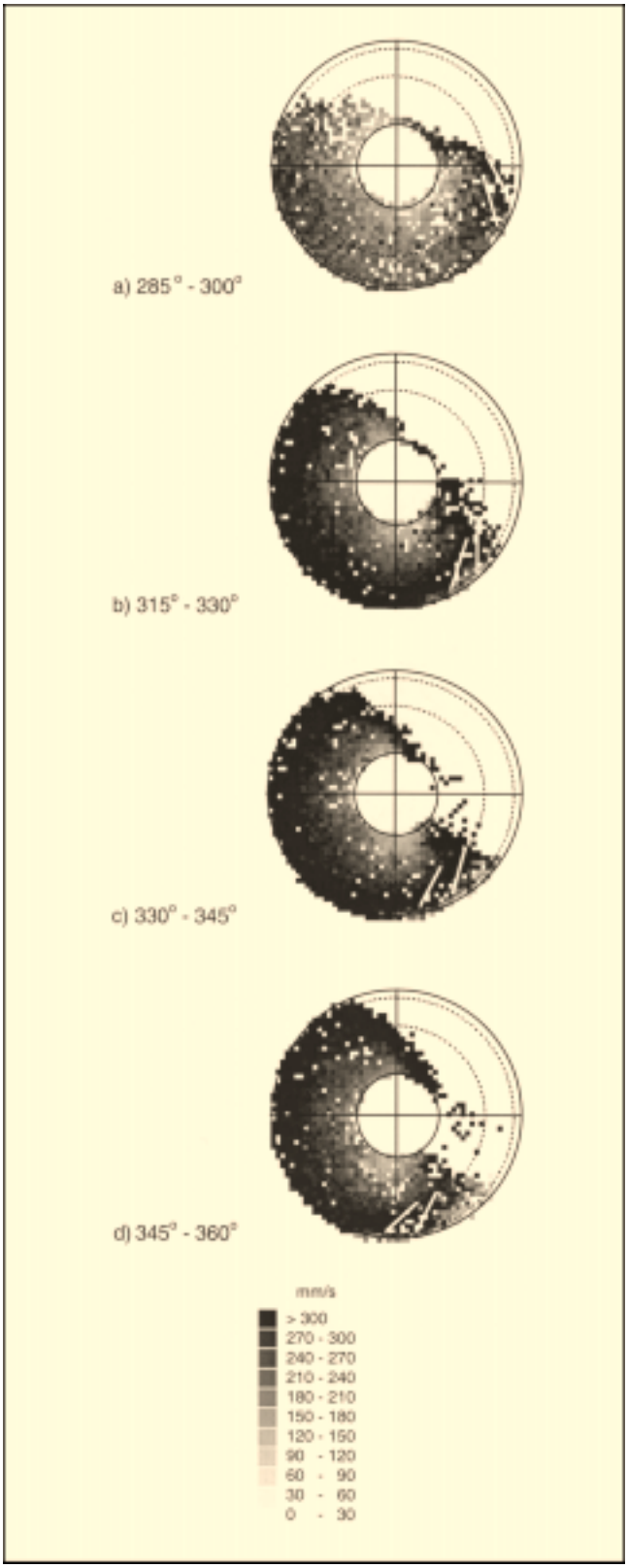

Figure 9. Profiles of the speed for different blade positions.

Cross-sectional view; level of fill—60%; $N = 38$ rpm.

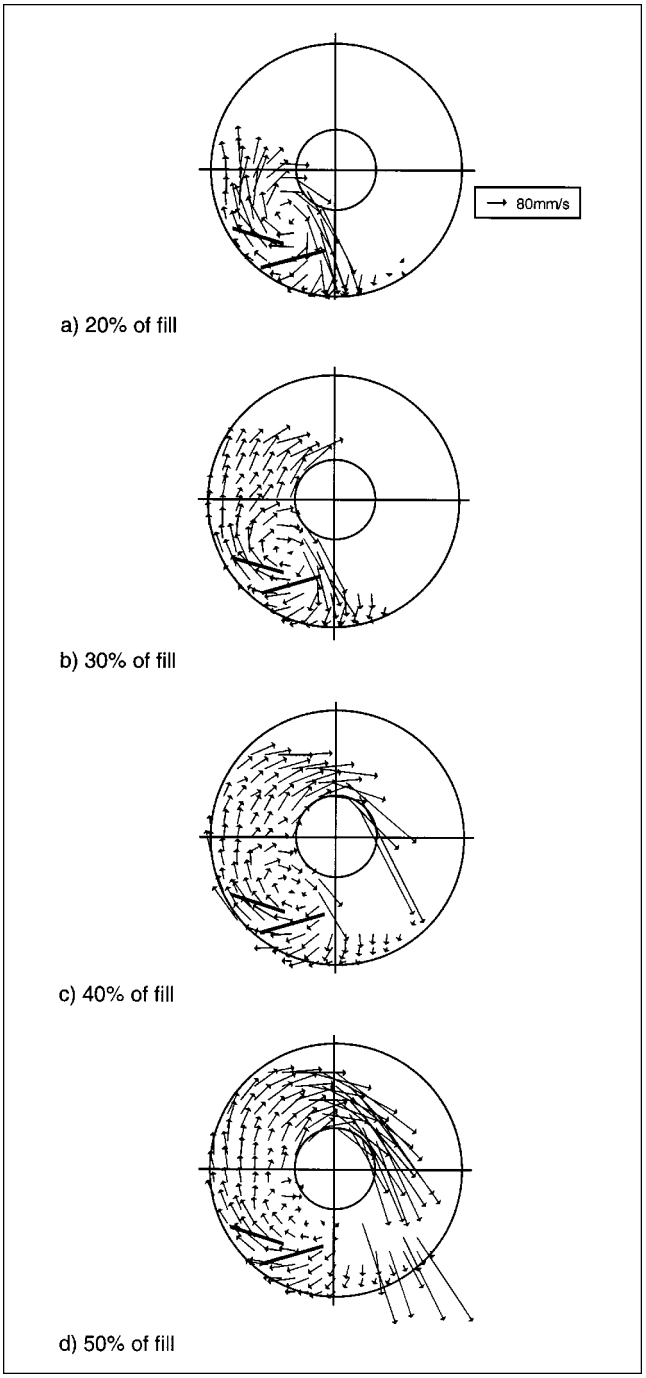

Figure 10. Velocity fields in cross-sectional view: $N = 38$ rpm.

Blade position between 30° and 60°.

from 0.06 to 0.31. This means gravity is more important than inertial forces in the range of agitator speeds investigated. It follows that the behavior of the bulk depends on the force exerted by the blade, frictional forces on the wall, shear forces, and gravity. The ratio of the mean tracer angular velocity to the agitator angular velocity was found to be approximately constant at 0.32 for the range of agitator speeds studied.

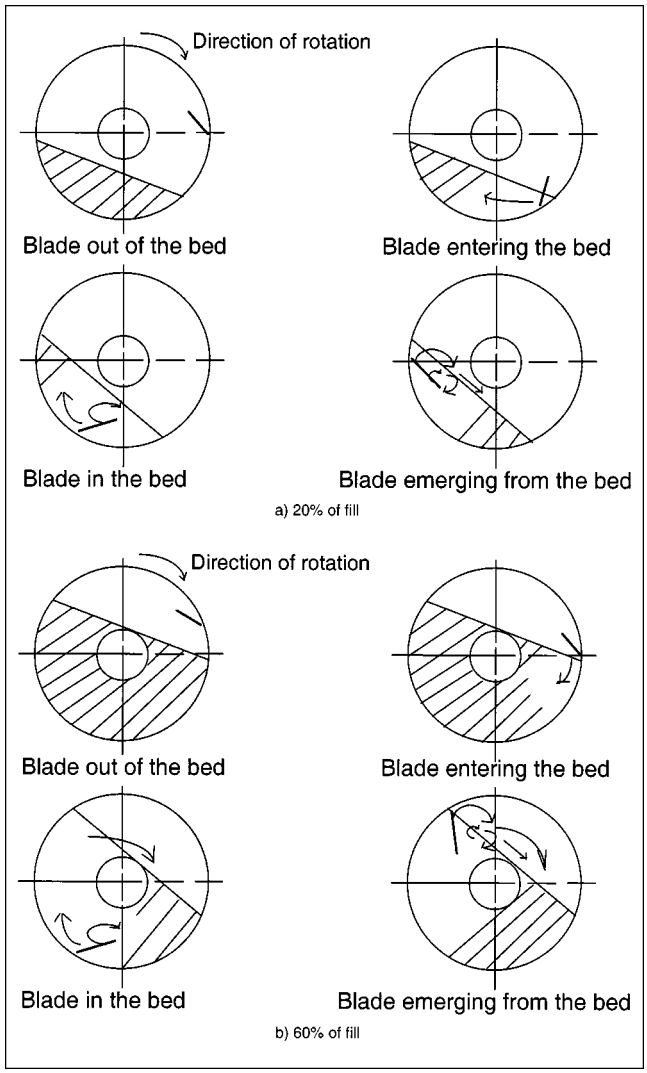

Figure 11. A blade cycle; transaxial flow patterns.

Stripes denote stationary zones.

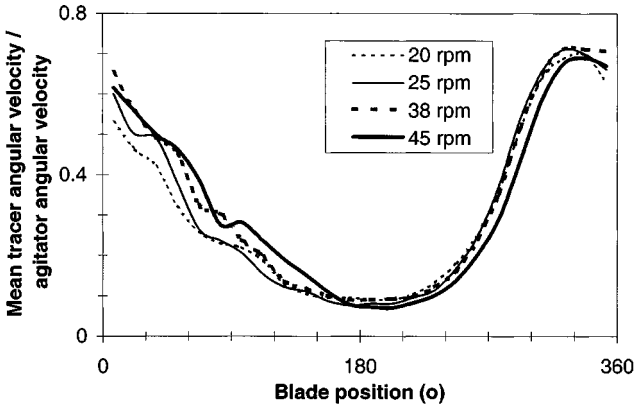

Figure 12. Influence of the agitator speed on the ratio of the mean tracer angular velocity of the tracer to the agitator angular speed.

Level of fill—60%.

Figure 13 presents $N_o \cdot P(N)$, the scaled power function of the Fourier transform $P(N)$ of the axial displacement of the tracer vs. the nondimensional frequency N/N_o, where N_o is the agitator speed, which varies between 20 and 45 rpm. This diagram shows the agitator speed-independence of the axial displacement, in agreement with results obtained by Miller et al. (1996), who measured stress fluctuations in an annular shear cell and showed that these were rate-independent when presented as scaled power functions. The present finding is to be linked with the ratio of the mean angular velocity to the agitator speed, which is independent of agitator speed. This evidence shows that the motion of the tracer and, subsequently, the powder flow patterns are dictated by the number of blade revolutions.

The peaks at a frequency of 1 and the subsequent harmonics at 2 and 3 correspond to an axial impulse at every blade pass through the bed. The peak at a frequency of 0.33 corresponds to the frequency of circulation of the tracer through the particle bed, as mentioned earlier. It appears at the same nondimensional frequency in the range of agitator speeds investigated. Thus means the number of blade passes needed to circulate the tracer through the bed from the bottom of the free surface back to the initial position is independent of the agitator speed and is, for example, around 3 for a level of fill of 60%.

At low frequencies, the spectra do not vary greatly. However, the spectra vary as $1/N$ at high frequency with a cutoff frequency of around 0.33, the frequency of circulation of the tracer through the particle bed. The $1/N$ dependence at high frequency of the spectra is somewhat analogous to that obtained in other dispersed systems. Savage (1991) predicted that the power spectra of stress fluctuations in the Couette flow of powder would obey such a law at high frequency. Miller et al. (1996) found a $1/N^2$ dependence by measuring stress fluctuations in an annular shear cell. Fauve et al. (1991) investigated avalanche processes in a rotating cylinder. They showed that the spectra of noises—which relate to the frequency and intensity of avalanches—also vary as $1/N^2$ at high frequency. These results are part of the more general trend $1/N^\alpha$ in dispersed systems, as Bak (1988) and Shlesinger and West (1988) showed in numerical simulation and analytical calculus, respectively. A $1/N^\alpha$ dependence represents an analogy with the "Kolmogorov-Obukov" $N^{-5/3}$ or the "Heisenberg" N^{-7} law of fluid turbulence.

Conclusions

The capability of the PEPT technique of investigating opaque media has been demonstrated. The information on the behavior of a single tracer particle having a similar size, shape, and density to that of mean bulk particles permitted the description of bulk flow patterns.

Investigations in a powder mixer of diameter 270 mm and length 650 mm using a long single blade of width 53 mm provides an understanding of the physics of flow in a simple system. At 20% of fill, the flow is directed only by the passage of the blade through the bed; the material cascades on the free surface and is recycled around a circulation loop situated immediately below the agitator shaft. This zone of lower agitation, characterized by low velocities, was found to decrease in size and to move toward the agitator shaft with an

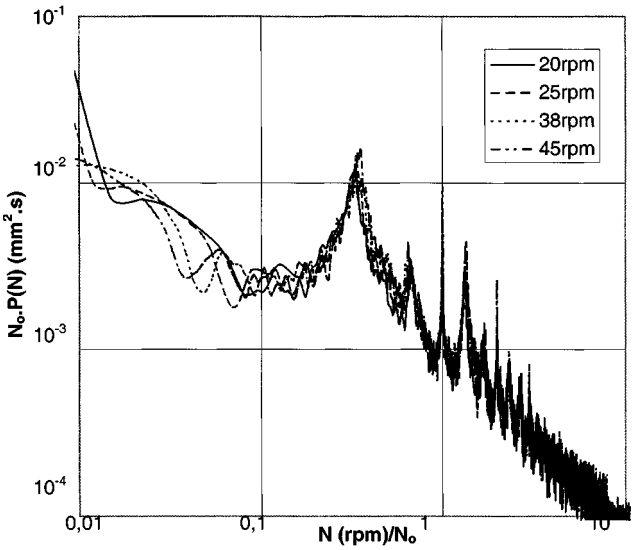

Figure 13. Influence of the agitator speed on the scaled power spectrum $N_o \cdot P(N)$ of the axial displacement.

Level of fill—60%.

increase of fill. The agitator shaft of diameter 90 mm does not interact with the material for levels of fill smaller than 30%. If the level of fill exceeds 30%, the shaft starts to play a part in the behavior, and for a fill of 60%, the bed is pushed by the blade like a plug through the channel between the agitator shaft and the mixer shell.

As the blade progresses into the particle bed, the torque increases, as does the mean velocity of the tracer. The torque is a maximum for a blade position corresponding closely to the maximum of the mean velocity.

Four blade passes brought the tracer from the bottom of the free surface to its top at a fill of 20%, this number decreasing to three at 60% of fill. This number was independent of speed for agitator speeds from 20 to 45 rpm, corresponding to a Froude number varying between 0.06 and 0.31. For the range of agitator speeds studied, the angular velocity scales with the agitator speed, implying that powder flow patterns are dictated by the number of blade passes. Data on axial displacement at various rotor speeds could be unified by the use of the scaled power functions of the Fourier transform of this displacement.

The experiments were performed on a mixer of one geometric design. If the vessel diameter were to be increased, with the blade remaining unchanged, it is probable the blade will disturb the material immediately above it, with the recycle behavior shown in Figure 4 occurring in the bulk. Material would continue to be placed onto the free surface, which can then cascade down the free surface, which lies below the rotor shaft at low levels of fill and above it at high levels of fill.

The wealth of information that is now available on internal flow structure has been demonstrated and could be readily incorporated in the existing models used in processing operations such as drying or agglomeration. This work has presented a methodology of investigation on a simple system from which we can now determine the radial and axial mixing behavior and this is being undertaken. The issue of geometric parameters (blade size and angle, number of blades, and vessel diameter) urgently needs attention to determine scale-up rules.

Acknowledgments

The authors thank Elf for their financial support. Thanks are also extended to D. Benton of the Positron Imaging Centre for his technical support. The authors are also grateful for the constructive comments of reviewers, in particular regarding the analysis of the power spectra of the tracer axial displacement.

Literature Cited

Bagster, D. F., and J. Bridgwater, ''The Flow of Granular Material over a Moving Blade,'' *Powder Technol.*, **3**, 323 (1970).

Bak, P., C. Tang, and K. Wiesenfeld, ''Scale Invariant Spacial and Temporal Fluctuations in Complex Systems,'' *Random Fluctuations and Pattern Growth: Experiments and Models*, H. E. Stanley and N. Ostrowsky, eds., NATO AS, Kluwer, Boston, MA, p. 329 (1988).

Broadbent, C. J., J. Bridgwater, D. J. Parker, S. T. Keningley, and P. Knight, ''A Phenomenological Study of a Batch Mixer Using a Positron Camera,'' *Powder Technol.*, **76**, 317 (1993).

Fauve, S., C. Laroche, and S. Douady, ''Dynamics of Avalances in a Rotating Cylinder,'' *Physics of Granular Media*, D. Bidear and J. Dodds, eds. Nova, Commack, NY, p. 343 (1991).

Khakhar, D. V., J. J. McCarthy, J. F. Gilchrist, and J. M. Ottino, ''Chaotic Mixing of Granular Materials in 2D Tumbling Mixers,'' *CHAOS*, **9**(1), 195 (1999).

Malhotra, K., A. S. Mujumdar, H. Imakoma, and M. Okazaki, ''Fundamental Particle Mixing Studies in an Agitated Bed of Granular Materials in a Cylindrical Vessel,'' *Powder Technol.*, **55**, 107 (1988).

Malhotra, K., and A. S. Mujumdar, ''Particle Mixing and Solids Flowability in Granular Beds Stirred by Paddle-Type Blades,'' *Powder Technol.*, **60**, 155 (1990).

McCarthy, J. J., T. Shinbrot, G. Metcalfe, J. E. Wolf, and J. M. Ottino, ''Mixing of Granular Materials in Slowly Rotated Containers,'' *AIChE J.*, **42**, 3351 (1995).

Metcalfe, G., G. Lachlan, K. Liffman, P. Cleary, and M. Shattuck, ''Imaging of Laboratory-Scale Industrial Granular Flows,'' *Proc. World Congress on Particle Technology 3*, Rugby, UK (1998).

Moakher, M., T. Shinbrot, and F. J. Muzzio, ''Experimentally Validated Computations of Flow, Mixing and Segregation of Non-Cohesive Grains in 3D Tumbling Blenders,'' *Powder Technol.*, **109**, 58 (2000).

Miller, B., C. O'Hern, and R. P. Behringer, ''Stress Fluctuations for Continuously Sheared Granular Materials,'' *Phys. Rev. Lett.*, **77**, 3110 (1996).

Müller, W., and H. Rumpf, ''Das Mischen von Pulvern in Mischern mit axialer Mischebewegung,'' *Chem.-Ing. Tech.*, **39**, 365 (1967).

Parker, D. J., C. J. Broadbent, P. Fowles, M. R. Hawkesworth, and P. McNeil, ''Positron Emitting Tracking—A Technique for Studying Flow within Engineering Equipment, *''Nucl. Instrum. Methods*, **326**, 592 (1993).

Parker, D. J., A. E. Dijkstra, T. W. Martin, and J. P. K. Seville, ''Positron Emission Particle Tracking Studies of Spherical Particle Motion in Rotating Drums,'' *Chem. Eng. Sci.*, **52**, 2011 (1997).

Poux, M., P. Fayolle, J. Bertrand, D. Bridoux, and J. Bousquet, ''Powder Mixing: Some Practical Rules Applied to Agitated Systems,'' *Powder Technol.*, **68**, 213 (1991).

Savage, S. B., ''Numerical Simulations of Couette Flow of Granular Material: Spatio-Temporal Coherence and 1/f Noise,'' *Physics of Granular Media*, D. Bidear and J. Dodds, eds., Nova, Commack, NY, p. 343 (1991).

Shinbrot, T., A. Alexander, M. Moakher, and F. J. Muzzio, ''Chaotic Granular Mixing,'' *CHAOS*, **9**, 611 (1999).

Shlesinger, M. F., and B. J. West, ''$1/f$ Versus $1/f^{\alpha}$ Noise,'' *Random Fluctuations and Pattern Growth: Experiments and Models*, H. E. Stanley and N. Ostrowsky, eds., NATO AS, Kluwer, Boston, MA, p. 329 (1988).

Manuscript received Jan. 18, 2000, and revision received May 1, 2000.